PAPER • OPEN ACCESS

Simulation of Alfvén eigenmodes destabilized by energetic electrons in tokamak plasmas

To cite this article: Jialei Wang *et al* 2020 *Nucl. Fusion* **60** 112012

OPEN ACCESS
IOP Publishing | International Atomic Energy Agency
Nuclear Fusion
Nucl. Fusion **60** (2020) 112012 (11pp)
https://doi.org/10.1088/1741-4326/ab6c79

Simulation of Alfvén eigenmodes destabilized by energetic electrons in tokamak plasmas

Jialei Wang[1,2], **Yasushi Todo**[2], **Hao Wang**[2] **and Zheng-Xiong Wang**[1]

[1] Key Laboratory of Materials Modification by Laser Ion, and Electron Beams (Ministry of Education), School of Physics, Dalian University of Technology, Dalian 116024, China
[2] National Institute for Fusion Science, National Institutes of Natural Sciences, Toki 509-5292, Japan

E-mail: zxwang@dlut.edu.cn

Received 6 November 2019, revised 25 December 2019
Accepted for publication 16 January 2020
Published 28 August 2020

Abstract

Alfvén eigenmodes (AEs) driven by energetic electrons were investigated via hybrid simulations of an MHD fluid interacting with energetic electrons. The investigation focused on AEs with the toroidal number $n = 4$. Both energetic electrons with centrally peaked beta profile and off-axis peaked profile are considered. For the centrally peaked energetic electron beta profile case, a toroidal Alfvén eigenmode (TAE) propagating in the electron diamagnetic drift direction is found. The mode is mainly driven by deeply trapped energetic electrons. It is also found that a few passing energetic electrons spatially localized around rational surfaces can resonate with the mode. For the off-axis peaked energetic electron beta profile case, an AE propagating in the ion diamagnetic drift direction is found when a $q-$profile with weak magnetic shear is adopted. The destabilized mode is an elliptical-Alfvén-eigenmode-type (EAE-type) mode which has a spatial profile peaking at the rational surface and a frequency close to the second Alfvén frequency gap. It is found that passing energetic electrons and barely trapped energetic electrons are responsible for this EAE-type mode destabilization. The saturation levels are compared for a TAE with the same linear growth rate among energetic electron driven mode and energetic ion driven mode with isotropic and anisotropic velocity space distributions. The saturation level of TAE driven by trapped energetic electrons is comparable to that driven by energetic electrons with isotropic velocity space distribution where the contribution of trapped particles is dominant. It is found that the trapped energetic ion driven TAE has a larger saturation level than the passing energetic ion driven TAE, which indicates the difference in particle trapping by the TAE between trapped and passing energetic ions.

Keywords: energetic electron, energetic ion, Alfvén eigenmode, wave-particle interaction, resonance condition

(Some figures may appear in colour only in the online journal)

1. Introduction

Alfvén eigenmodes (AEs) are magnetohydrodynamic (MHD) oscillations of the non-uniform magnetically confined plasmas [1–4]. AEs are intrinsically stable but can be excited by energetic particles via the wave-particle resonance [5]. In burning plasmas, energetic particles (both ions and electrons) will be abundantly produced by high-power heating and fusion reactions. The excited AEs are one of the major concerns of

burning plasmas because they can transport alpha particles and reduce the alpha heating efficiency leading to a deterioration of fusion reactor performance [6]. Therefore, it is crucial to understand instabilities driven by alphas or other energetic particles. In the past decades, experimental, theoretical and numerical studies of the interaction between AEs and energetic ions which are accelerated by neutral beam injection (NBI) and ion cyclotron resonance frequency (ICRF) heating, have been extensively conducted in tokamaks, stellarators and heliotrons [7–18]. By contrast, far less attention has been paid to energetic-electron driven instabilities. Indeed, the study of energetic electrons is important not only for understanding its own behavior in driving Alfvén instabilities, but also for understanding the behavior of alpha particles in burning plasmas [7, 19, 20].

AEs destabilized by energetic electrons have been observed in several devices with high-power electron cyclotron wave (ECW) or lower hybrid wave (LHW) heating. AEs destabilized by energetic electrons was first observed on COMPASS-D during electron-cyclotron resonance heating (ECRH) [21]. In HL-2A, mode features of energetic-electron driven beta-induced Alfvén eigenmode (BAE) and toroidal Alfvén eigenmode (TAE) were analysed during ECRH [22–24]. These destabilized modes during ECRH mainly propagate in the electron diamagnetic drift direction. Energetic electrons generated by LHW can also destabilize AEs [25, 26]. In EAST LHW experiment [26], the observed AEs can propagate in either ion or electron diamagnetic drift direction. In addition, it was recently reported that energetic electrons induced by static magnetic perturbations can also drive a TAE propagating in the ion diamagnetic drift direction [27]. These experimental studies revealed some properties of energetic-electron driven AE, including its frequency, mode number and propagation direction. The different propagation directions observed in experiments also suggest that different types of energetic electrons can drive the AEs. However, the exact destabilization mechanism of AEs by energetic electrons is not clear. Computer simulation provides a powerful tool to investigate the detailed interaction between AEs and energetic particles. The destabilization of energetic-electron driven BAE was reproduced numerically for the first time using gyrokinetic toroidal code (GTC) [28], but other AEs, such as TAE and ellipticity-induced Alfvén eigenmode (EAE), driven by energetic electrons have not been demonstrated numerically yet. The nonlinear evolution of energetic-electron driven AE is another area worthy of analysis. Therefore, a comprehensive understanding of linear and non-linear properties of energetic-electron driven AEs motivates us to conduct this work.

The analogies between energetic electrons in present-day devices and alpha particles in burning plasmas further motivate us to investigate the interaction between AEs and energetic electrons. In present devices, passing energetic ions can be used to study the interaction with AEs and associated ion transport for ITER relevant energy and orbit characteristics [7]. However, trapped energetic ions are expected to have small dimensionless orbits in burning plasmas due to the large plasma current in these devices [7, 19, 20], while trapped ions in present-day experiments have much larger orbits. The small orbits of energetic ions in burning plasmas are similar to energetic electrons in present-day experiments. In other words, energetic electrons provide a complementary tool to investigate wave-particle interactions relevant for burning plasmas in present devices.

In this work, the destabilization of AE with a single toroidal mode number $n = 4$ by energetic electrons is numerically studied using MEGA code [29–33], which is a hybrid simulation code for energetic particles interacting with an MHD fluid. Both centrally peaked and off-axis peaked energetic electron beta profiles are adopted in order to destabilize the AEs propagating in the electron/ion diamagnetic drift direction. It is found that TAE propagating in the electron diamagnetic drift direction can be excited by deeply trapped energetic electrons with a centrally peaked profile, while a few passing energetic electrons spatially localized around rational surfaces can also resonate with the mode. It is also found that the TAE frequency will increase when initial loading energetic electrons have higher energy. Besides, a comparison of nonlinear saturation levels of the energetic-electron driven TAE and energetic-ion driven TAE is conducted. It shows that the energetic-electron driven TAE and energetic-ion driven TAE with the same linear growth rate have the similar saturation level. For off-axis energetic electron profile with weak magnetic shear at the mode center, an EAE-type energetic particle mode (EAE-type EPM) propagating in the ion diamagnetic drift direction is successfully excited. The mode is driven by passing and barely trapped energetic electrons. The detailed wave-particle resonance condition and power transfer will be presented. The remainder of this paper is organized as follows. In section 2, the simulation model is introduced. In section 3, the numerical results are presented. In the final section 4, we summarize and discuss the results.

2. Physical model

Several hybrid simulation models have been constructed to study the evolution of AE modes destabilized by energetic particles [29, 34–37]. In the MEGA code, the bulk plasma is described by the non-linear MHD equations and the energetic particles described by drift-kinetic equations are simulated with the particle-in-cell method. The MHD equations with the energetic particle effects are given by

$$\frac{\partial \rho}{\partial t} = -\nabla \cdot (\rho \boldsymbol{v}) + \nu_n \Delta (\rho - \rho_{\rm eq}), \tag{1}$$

$$\rho \frac{\partial \boldsymbol{v}}{\partial t} = -\rho \boldsymbol{\omega} \times \boldsymbol{v} - \rho \nabla \left(\frac{v^2}{2} \right) - \nabla p + (\boldsymbol{j} - \boldsymbol{j}_h) \times \boldsymbol{B} + \frac{4}{3} \nabla (\nu \rho \nabla \cdot \boldsymbol{v}) - \nabla \times (\nu \rho \boldsymbol{\omega}), \tag{2}$$

$$\frac{\partial p}{\partial t} = -\nabla \cdot (p \boldsymbol{v}) - (\gamma - 1) p \nabla \cdot \boldsymbol{v} + (\gamma - 1) \left[\nu \rho \omega^2 + \frac{4}{3} \nu \rho (\nabla \cdot \boldsymbol{v})^2 + \eta \boldsymbol{j} \cdot (\boldsymbol{j} - \boldsymbol{j}_{\rm eq}) \right] + \chi \Delta (p - p_{\rm eq}), \tag{3}$$

$$\frac{\partial \boldsymbol{B}}{\partial t} = -\nabla \times \boldsymbol{E}, \boldsymbol{j} = \frac{1}{\mu_0}\nabla \times \boldsymbol{B}, \tag{4}$$

$$\boldsymbol{E} = -\boldsymbol{v} \times \boldsymbol{B} + \eta\left(\boldsymbol{j} - \boldsymbol{j}_{\mathrm{eq}}\right), \tag{5}$$

$$\boldsymbol{\omega} = \nabla \times \boldsymbol{v}, \tag{6}$$

where μ_0 is the vacuum magnetic permeability, $\gamma = 5/3$ is the adiabatic constant, ν, ν_n and χ are artificial viscosity and diffusion coefficients chosen to maintain numerical stability, and all the other quantities are conventional. The subscript 'eq' and 'h' denote the equilibrium variables and the energetic particles, respectively. In this work, we use the same value of the dissipation coefficients, 1×10^{-6} normalized by $v_{\mathrm{A}}R_0$ where v_{A} is the Alfvén velocity at the plasma center, and R_0 is the major radius at the geometrical center of the simulation domain. The energetic particle contribution is included in the MHD momentum equation (equation (2)) as the energetic particle current density without $\boldsymbol{E} \times \boldsymbol{B}$ drift due to the quasi-neutrality [20]. This model is accurate under the condition that the energetic particle density is much less than the bulk plasma density.

The MHD equations are solved using standard 4th order Runge–Kutta and finite difference schemes. The non-relativistic drift-kinetic description [38] is employed for energetic particles. The computational particles are initially loaded uniformly in the phase space. A detailed description of model equations and numerical methods can be found in [29, 30]. MEGA code participated in the code benchmark of the Energetic Particle Physics Topical Group of the International Tokamak Physics Activity. Good agreements were found in the spatial profile, mode frequency and growth rate of a TAE among nine codes including MEGA [39]. The MEGA code has been applied to and validated on the energetic-particle driven instabilities in several devices, such as LHD, JT-60U and DIII-D [40–44].

A tokamak plasma with aspect ratio of $R_0/a = 3.2$ was investigated where a is the plasma minor radius. MHD fields and kinetic particles are both evolved in right-handed cylindrical coordinates (R, φ, Z). The shape of the outermost magnetic surface is circular. Spatial profiles of energetic particle beta and safety factor are shown in figure 1. Both centrally peaked and off-axis peaked energetic particle beta profiles are investigated. It should be noted that a uniform bulk plasma beta profile with an initial value of 1% is adopted here in order to avoid/mitigate some pressure gradient driven instabilities. The safety factor profile, unless otherwise explicitly stated, is assumed to be the same as in [31], $q = 1 + 2(r/a)^2$. The Maxwellian distribution function is used as the initial velocity-space distribution of energetic particles:

$$f_h = C\left(\frac{m_{\mathrm{h}}}{\mathrm{T_h}}\right)^{3/2} e^{-m_{\mathrm{h}}v^2/2\mathrm{T_h}} \cdot g(\Lambda), \tag{7}$$

where C is an integration constant. The uniform temperature $\mathrm{T_h}$ is adopted for simplicity, which is normalized by $m_{\mathrm{D}}v_A^2$

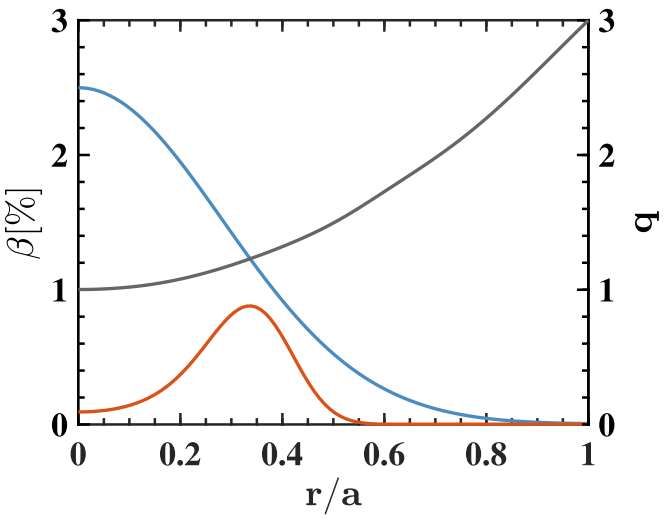

Figure 1. Spatial profiles of energetic-particle beta peaked on-axis (blue curve), energetic-particle beta peaked off-axis (orange curve) and safety factor (dark curve).

where m_{D} is the mass of energetic deuteron ion. The pitch angle distribution is $g(\Lambda) = 1$ for isotropic Maxwellian distribution and $g(\Lambda) = \exp[-(\Lambda - \Lambda_{peak})^2/\Delta\Lambda^2]$ for anisotropic Maxwellian distribution, respectively. $\Lambda = \mu B_0/E$ is the pitch angle variable with the B_0 magnetic field strength at the magnetic axis. The pitch angle width $\Delta\Lambda$ is set to 0.3 in this work. The ratio of the minor radius to the energetic-ion Larmor radius is 16 for the energetic ion velocity equal to the Alfvén velocity. The normalized mass of the energetic particle m_{h} is set to 1/3672 for energetic-electron simulations and 1 for energetic-ion simulations. The finite Larmor radius effect for the energetic particles is neglected. In the present work, we focus on 'single-n' simulations, where energetic particles drive only one toroidal mode number n. The evolution of $n = 4$ mode, which is an exact solution of the equations of a quarter of the tokamak domain in toroidal direction, is investigated. Then, only the toroidal angle from $\varphi = 0$ to $\varphi = \pi/2$ is used for the present simulation, while toroidal angle from $\varphi = \pi/2$ to $\varphi = 2\pi$ are obtained by periodic extension. This simplification is made to save computational resources and time compared with a full torus simulation. The number of grid points for the cylindrical coordinates (R, φ, Z) is $128 \times 64 \times 128$ and the number of computational particles is 8.4×10^6.

3. Simulation results

We conducted two types of simulations using centrally peaked and off-axis peaked energetic electron beta profiles. For the AE destabilized by energetic particle spatial gradient, the toroidal propagation direction is determined by the sign of the energetic particle charge (e_h), the radial derivative of the energetic particle distribution function $(\partial f/\partial r)$, and the poloidal magnetic field (B_θ) [45]. When $\mathrm{sign}(e_h) \cdot \mathrm{sign}(\partial f/\partial r) \cdot \mathrm{sign}(B_\theta) = 1$, the mode propagates in $+\varphi$ direction. The poloidal propagation will be determined from the toroidal propagation through the sign of m/n, where m is the poloidal

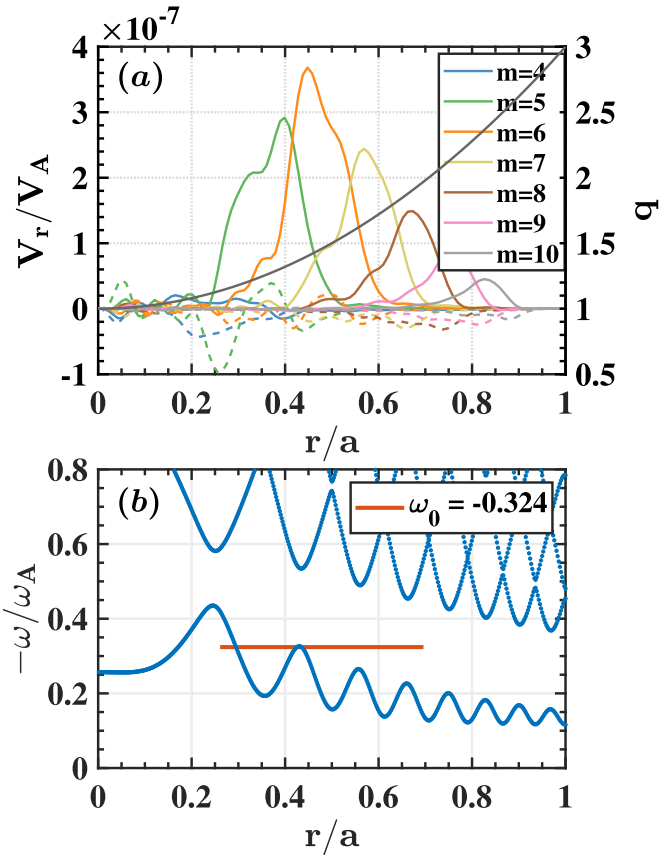

Figure 2. (*a*) Radial velocity fluctuation profiles of TAE with toroidal mode number $n=4$. (*b*) Alfvén continuous spectra for $n=4$. Solid (dashed) lines in (*a*) show $\cos(m\theta+n\varphi)$ $[\sin(m\theta+n\varphi)]$ harmonics with poloidal mode number m listed in the figure. Frequency and spatial location of the $n=4$ TAE are shown in (*b*) with the horizontal line. A centrally peaked energetic electron beta profile is adopted. $\omega_A=v_A/R_{\rm axis}$, where $R_{\rm axis}$ is the major raidus of the magnetic axis. The energetic electron temperature is $\mathrm{T_h}=0.3$.

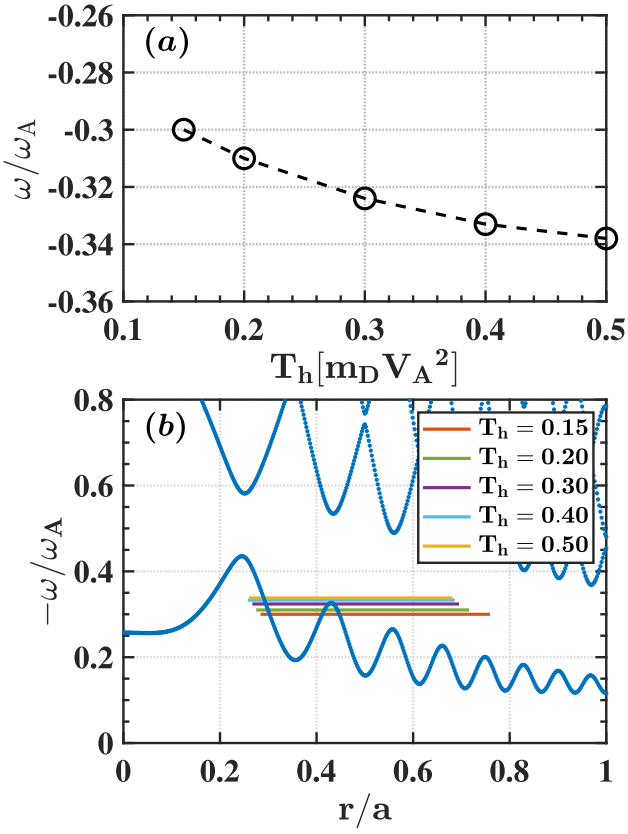

Figure 3. (*a*) Mode frequency versus the energetic electron temperature $\mathrm{T_h}$. (*b*) Alfvén continuous spectra for $n=4$. The energetic electron beta profile holds fixed in the scan of $\mathrm{T_h}$. Frequencies and spatial locations of the $n=4$ modes are shown in (*b*) with the horizontal lines.

mode number. The plasma current in this work is in $+\varphi$ direction $[\mathrm{sign}(B_\theta)=-1]$. Then, a centrally/off-axis peaked energetic electron beta profile with $\mathrm{sign}(\partial f/\partial r)=-1$ at the mode center could drive an AE propagating in the electron diamagnetic drift direction, which will be presented in subsections 3.1 and 3.2, while an off-axis peaked energetic electron beta profile with $\mathrm{sign}(\partial f/\partial r)=1$ at the mode center could drive an AE propagating in the ion diamagnetic drift direction, which will be presented in subsection 3.3. In subsection 3.4, finally, we will discuss the non-linear saturation levels of energetic-electron driven TAE and energetic-ion driven TAE with similar initial energetic particle distributions.

3.1. Energetic electrons with beta profile peaked on-axis $(\partial f/\partial r<0)$

The spatial profile and mode frequency of energetic-electron driven $n=4$ TAE are shown in figure 2. The initial velocity-space distribution of energetic electrons is isotropic Maxwellian distribution with $\mathrm{T_h}=0.3$. The equilibrium profiles and simulation parameters adopted here are similar to the previous work for investigating non-linear MHD effects on the evolution of energetic-ion driven TAE [31]. The mode shows two major harmonics $(m,m+1)/n=(5,6)/4$ which peaked around $q=(5+1/2)/4$. Other poloidal harmonics with $m\geq 7$ also appear because a wide energetic electron beta profile is used. The mode frequency shown in figure 2(*b*) is around the extremum of the lower Alfvén continuum, which indicates the dominant fluctuations are TAE mode. The slow sound approximation [46] is adopted for the Alfvén continua analysis, and the MHD pressure used in the analysis is the sum of thermal pressure and energetic particle pressure. The negative sign of TAE frequency indicates that the mode propagates in the electron diamagnetic drift direction, which is consistent with theoretical prediction as already introduced previously.

According to previous studies on energetic-electron driven modes with the negative frequency, such as e-fishbone [19, 20] r19, r20, r47 and r48 and e-BAE [28], deeply trapped energetic electrons are expected to drive those modes through precession resonance. The precession frequency of an energetic particle is proportional to its kinetic energy [47]. This suggests that the linear property of energetic-electron driven TAE may have a strong relation with the energetic electron energy. The dependence of TAE frequency and spatial location on energetic electron temperature is shown in figure 3. We see clearly that the mode frequency (absolute value) increases when the energetic

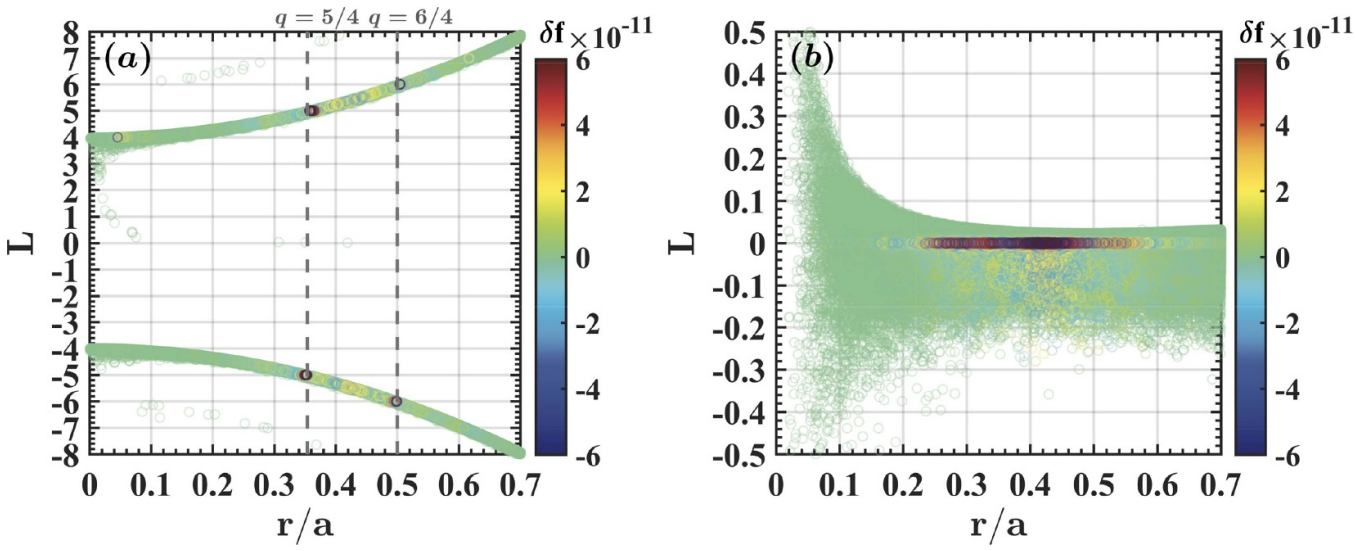

Figure 4. Resonance condition for (*a*) passing energetic electrons and (*b*) trapped energetic electrons along radial coordinate. Each marker in the figure represents one computational particle and all particles are included. Particle positions in the mid-plane during one bounce/transit period are stored and the average value of the stored positions is used as the particle location in the figure.

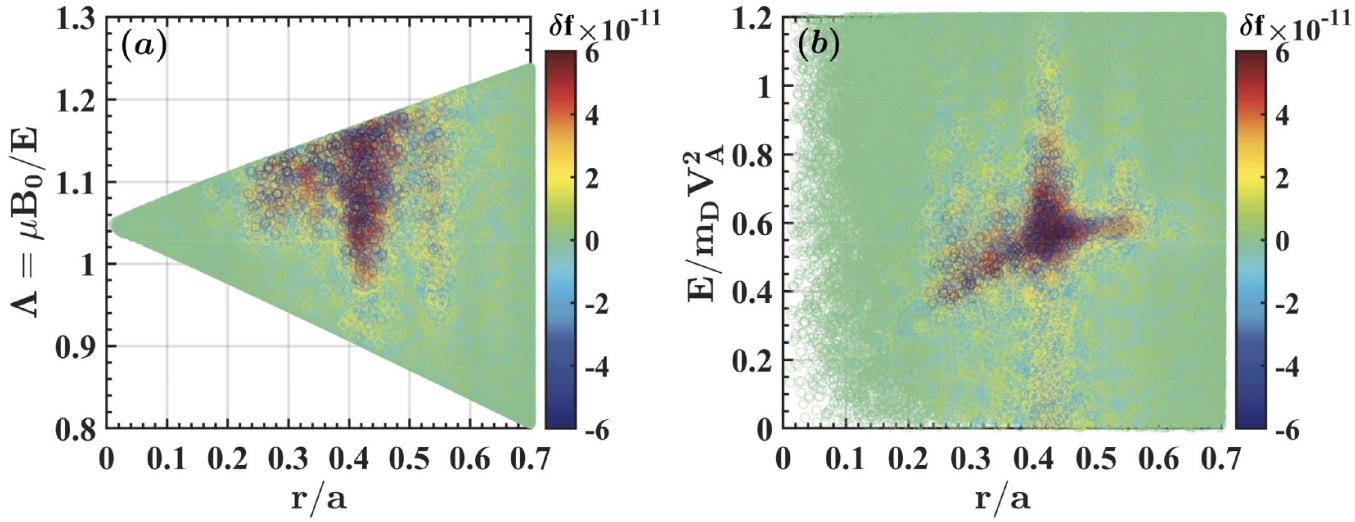

Figure 5. Phase space (*a*) (r, Λ) and (*b*) (r, E) structures of δf for trapped energetic electrons in the linear phase.

electron temperature increases from 0.15 to 0.5, and the variation rate of mode frequency becomes small at large temperature values. Besides, the radial location of the mode slightly moves inward with the increase of temperature as shown in figure 3(*b*). It should be noted that no unstable mode was found for the case with $T_h = 0.1$. From the trend in figure 3, the mode frequency (absolute value) at $T_h = 0.1$ is expected to further decrease than the case with $T_h = 0.15$ and the mode will suffer the stronger continuum damping [48, 49]. As a result, a higher energetic electron beta is needed to excite the mode at $T_h = 0.1$.

In order to confirm the destabilization mechanism of energetic-electron driven TAE, the resonance condition and the power transfer between energetic electrons and the mode are analysed. The resonance condition for a low frequency wave (mode frequency much less than the cyclotron frequency) in a torus is [50]

$$\omega_0 - L\omega_\theta - n\omega_\varphi = 0, \tag{8}$$

where ω_0 is the mode frequency, and integer L is the resonance number. ω_θ and ω_φ are particle poloidal and toroidal orbit frequency, respectively. Figures 4(*a*) and (*b*) show the resonance condition for all passing and trapped energetic electrons, respectively. Particles with large value of $|\delta f|$ indicate a strong interaction with the mode. It is found that the dominant resonance numbers for passing particles are $L = \pm 5$ and $L = \pm 6$. The radial region of these resonant passing-particles is closely around the rational surface $q = 5/4$ and $q = 6/4$. Due to the small value of the parallel wave vector $k_{||}$ near the rational surface, passing energetic electrons even with large orbit frequencies (compared to the mode frequency) can resonate with the shear Alfvén wave (SAW). Trapped energetic electrons shown in figure 4(*b*), contrary to passing energetic electrons, can resonate with the mode at a wide range of minor radius

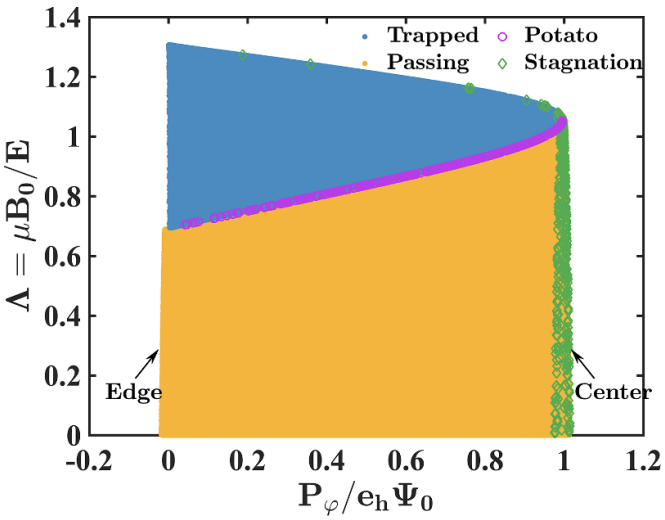

Figure 6. Energetic electron distribution in (P_φ, Λ) space in the linear phase. It should be noted that some particles indicated as Potato in the figure do not have a steady potato orbit. The orbit types of these particles convert among potato, passing and barely trapped.

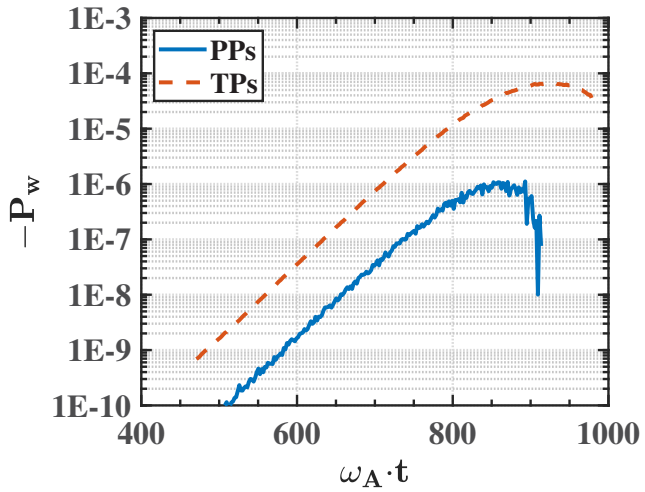

Figure 7. Evolution of phase space integrated power transfer from passing energetic electrons (blue solid) and trapped energetic electrons (red dashed) to the TAE. 'PPs' ['TPs'] is an abbreviation of 'passing particles' ['trapped particles'].

through precession resonance with $L=0$. The pitch angle information for trapped energetic electrons is shown in figure 5(a). The lower boundary in the figure indicates the separatrix between trapped and passing particles. Trapped particles close to the lower and upper boundaries are barely trapped and deeply trapped particles, respectively. Thus, it is confirmed in figure 5(a) that most of resonant energetic electrons are deeply trapped particles. The kinetic energy of trapped energetic electrons with large $|\delta f|$ is mainly between $0.4\,m_D v_A^2$ and $0.6\,m_D v_A^2$, as shown in figure 5(b). In addition, the energetic electrons considered in the present case are actually quite large and the large particle energy may lead to a non-conventional orbit (stagnation or potato). The energetic electron orbits were carefully examined and the particle distribution in (P_φ, Λ) space is shown in figure 6. Toroidal canonical momentum is given by $P_\varphi = e_h\Psi + m_h R b_\varphi v_\parallel$, where Ψ is the poloidal magnetic flux with $\Psi = \Psi_0$ at the plasma center and $\Psi = 0$ at the edge, and b_φ is the φ component of the unit vector of magnetic filed. Only a tiny fraction of non-conventional particles (about 0.01% of all particles) are found and few of them are resonating with the mode as most of non-conventional electrons lies outside of the TAE. The contribution from the non-conventional electrons can be neglected. Besides, we see in figure 4 that some non-resonant energetic electrons (non-integer L) around the mode center ($r/a \sim 0.4$) also have large values of $|\delta f|$, but the net power transfer from these particles is also negligible.

The power transfer of energetic electrons due to the wave-particle interaction is computed as

$$P_w(\boldsymbol{x},\boldsymbol{v}) = \sum_{i=1}^{N} \frac{dE_i}{dt} w_i S(\boldsymbol{x}-\boldsymbol{x}_i, \boldsymbol{v}-\boldsymbol{v}_i), \tag{9}$$

where N is the total number of particles, dE_i/dt is the time derivation of the kinetic energy, w_i is the particle weight, and S is the 0th-order shape factor in order to select particles with specific characteristics in phase space. The particles drive the mode when $P_w < 0$, vice versa. The net power transfer from trapped and passing energetic electrons to the TAE is shown in figure 7. Trapped energetic electrons accounts for about 90% of the total power transfer in the linear phase. The net power transfer from passing particles is little, because the resonance region, as already shown above, is very spatially localized for the $q-$profile adopted here, which restricts the number of resonant passing-energetic-electrons. Conversely, passing energetic electrons seem to become important in a weak magnetic shear plasma as more passing energetic electrons can interact with the mode. The relevant results will be shown in subsection 3.3.

3.2. Energetic electrons with beta profile peaked off-axis ($\partial f/\partial r < 0$)

The wave growth in this work is driven by the free energy stored in spatial gradient of energetic particle distribution function. An off-axis peaked energetic electron beta profile at a value of 0.88% with large spatial gradient, which is denoted by orange solid line in figure 1, can also drive a TAE. The initial velocity-space distribution of energetic electrons is still isotropic Maxwellian distribution with $T_h = 0.3$ and other equilibrium profiles and parameters are the same as those in subsection 3.1. Figure 8 shows the spatial profiles and Alfvén continuous spectra for the unstable TAE. The major harmonics are still $(m, m+1)/n = (5, 6)/4$, but poloidal harmonics $m \geq 7$ are strongly damped or disappear compared to the case with a wide centrally-peaked energetic electron beta profile used in figure 2. The propagation of the mode remains in the electron diamagnetic drift direction as the spatial gradient of energetic electron distribution function $\partial f/\partial r$ is still negative at the mode center ($r/a \sim 0.43$).

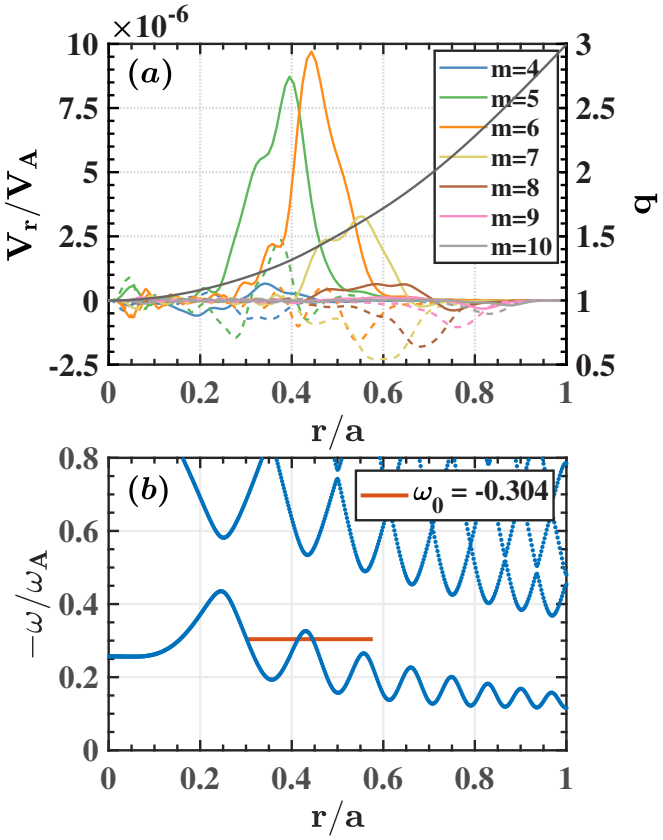

Figure 8. (*a*) Radial velocity fluctuation profiles of TAE with toroidal mode number $n = 4$. (*b*) Alfvén continuous spectra for $n = 4$. An off-axis peaked energetic electron beta profile is adopted.

3.3. Energetic electrons with beta profile peaked off-axis $(\partial f/\partial r > 0)$

To further understand the role of passing energetic electrons in driving the AE, another simulation with weak magnetic shear at the core region has been carried out. Equilibrium profiles of bulk plasma beta, energetic electron beta and safety factor used in this subsection are shown in figure 9. Safety factor in the core region is around $q = 7/4$, where the precise position of $q = 7/4$ rational surface is at $r/a = 0.283$, as the dashed line shown in figure 9. The spatial gradient of energetic electron distribution function at $q = 7/4$ rational surface is positive $(\partial f/\partial r > 0)$ and the initial velocity-space distribution of energetic electrons is still isotropic Maxwellian distribution with $T_h = 0.3$.

An unstable AE driven by energetic electrons with $\partial f/\partial r > 0$ was found. Figure 10 shows the spatial profiles and continuous spectra for the unstable mode. This energetic-electron driven mode locating around $q = 7/4$ rational surface has two major poloidal harmonics $m = 6$ and $m = 8$, but the imaginary part of $m = 8$ is also large. The mode is intersecting the continuum at a frequency $\omega_0 = 0.549\omega_A$. The positive value of frequency indicates that the mode propagates in the ion diamagnetic drift direction. The dominant poloidal number of the unstable mode resembles the so-called EAE, which is also characterized by two dominant poloidal harmonics m and

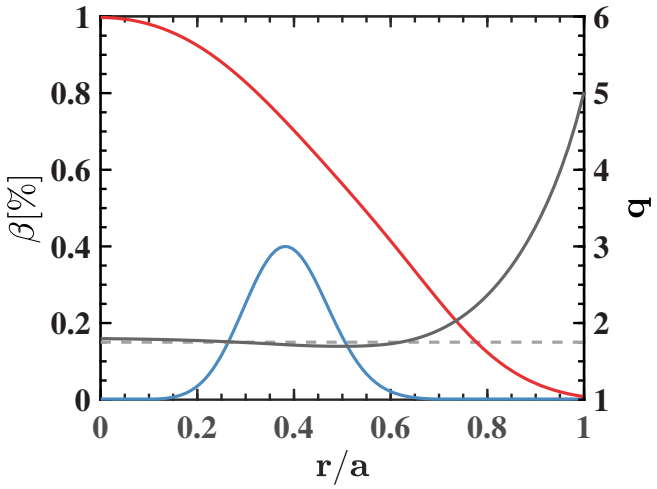

Figure 9. Spatial profiles of energetic-particle beta peaked off-axis (blue curve), bulk plasma beta (red curve) and safety factor (dark curve). The dark dashed line indicates the safety factor $q = 7/4$.

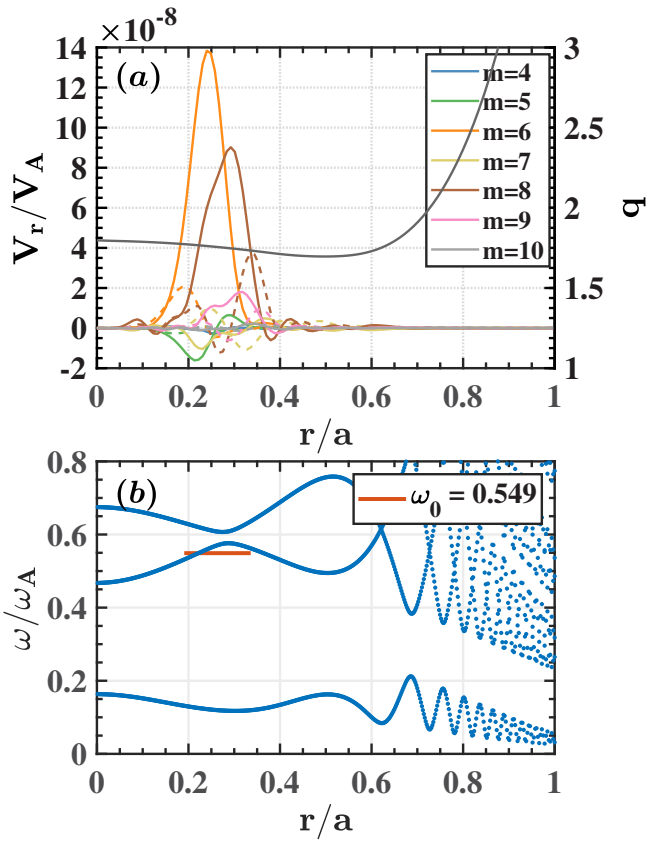

Figure 10. (*a*) Radial velocity fluctuation profiles of EAE-type EPM with toroidal mode number $n = 4$. (*b*) Alfvén continuous spectra for $n = 4$.

$m + 2$. However, the EAE frequency lies in the second Alfvén frequency gap, while the frequency of the unstable mode here lies below the second Alfvén frequency gap due to the narrow second gap for present circular cross-section plasmas. Then, we would call this unstable mode as an EAE-type EPM.

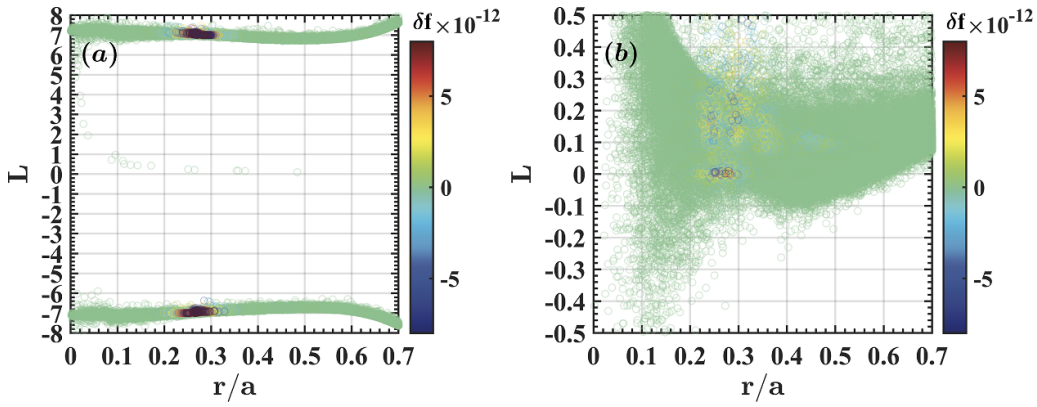

Figure 11. Resonance condition for (a) passing energetic electrons and (b) trapped energetic electrons along the radial coordinate.

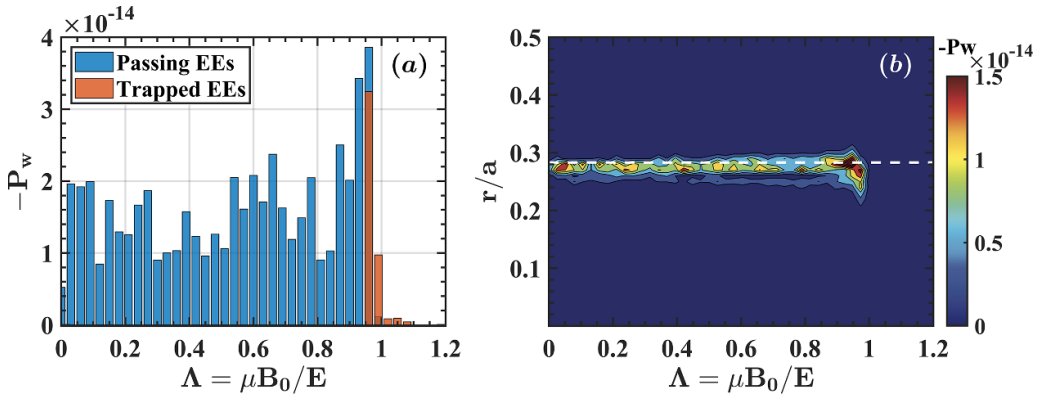

Figure 12. (a) Power transfer from energetic electrons characterized by pitch angle Λ to the EAE-type EPM . (b) phase space (Λ, r) structure of power transfer from energetic electrons to the mode. The white dashed line in (b) indicates the radial position of $q = 7/4$ rational surface. 'EE' ['EI'] is an abbreviation of 'energetic electron' ['energetic ion'].

Figures 11(a) and (b) show the resonance condition of passing and trapped energetic electrons with the EAE-type EPM, respectively. Passing energetic electrons are resonating with the resonance number $L = \pm 7$, while trapped energetic electrons are resonating through precession resonance with $L = 0$. Due to the flat $q-$profile around the mode center ($r/a = 0.283$), we see in figure 11(a) that passing energetic electrons can resonate with the mode at a wide radial region, which is about 10% of the plasma minor radius a. In addition, considering the positive mode frequency, the precession drift frequency of resonant trapped-energetic-electron should also be positive in order to match the resonance condition with $L = 0$.

The power transfer between energetic electrons and the EAE-type EPM is analysed in (Λ, r) space. Figure 12(a) shows the power transfer of energetic electrons characterized by particle pitch angle Λ. The power transfer of passing energetic electrons with different pitch angle is similar except the particles near passing/trapped boundary with a large value of Λ. On the contrary, the power transfer of trapped energetic electrons has a strong dependence on the particle pitch angle and most of drive comes from the particles with $\Lambda < 1$. Moreover, the small pitch angle value and positive precession drift frequency of the resonant trapped-energetic-electrons confirms these particles are barely trapped energetic electrons. Figure 12(b) shows the power transfer of all computational particles in (Λ, r) space. The radial region where the power transfer is large changes little when energetic electrons are away from the passing/trapped boundary, and the power transfer region broadens when energetic electrons are around the passing/trapped boundary.

It should be noted that the significant role of passing energetic electrons in destabilizing the EAE-type EPM can not be applied to the TAE in a weak magnetic shear plasma. The drive from passing energetic electrons in destabilizing TAE is often far from sufficient to overcome the damping, even a large energetic electron beta is used. The small drive of passing energetic electrons in destabilizing TAE can be understood as follows. First, if there are wave-particle interactions between a TAE and passing energetic electrons at the rational surface $q = (m + 1/2)/n$, it would lead to a fractional value of resonance number L; and second, energetic electron drift orbit width is very small and the adjacent rational surfaces $q = m/n$ and $q = (m + 1)/n$ will be far away from the mode center $q = (m + 1/2)/n$ due to the weak magnetic shear unless a very high n is considered, then passing energetic electrons at these two adjacent rational surfaces, m/n and $(m + 1)/n$, are still difficult to resonate with the mode.

Table 1. Numerical parameters for cases (I–V) studied in subsection 3.4. The mode frequency is also listed. The centrally peaked energetic particle beta profile with an initial value of β_h is adopted. The linear growth rates for cases (I–V) are the same $\gamma_L/\omega_A = 0.028$.

Case	EP	$\beta_h[\%]$	$g(\Lambda)$	Λ_{peak}	$\Delta\Lambda$	ω_0/ω_A
(I)	EE	3.30	Isotropic	-	-	0.308
(II)	EE	1.73	Anisotropic	1.0	0.3	0.324
(III)	EI	1.86	Isotropic	-	-	0.359
(IV)	EI	1.84	Anisotropic	1.0	0.3	0.352
(V)	EI	1.63	Anisotropic	0.3	0.3	0.362

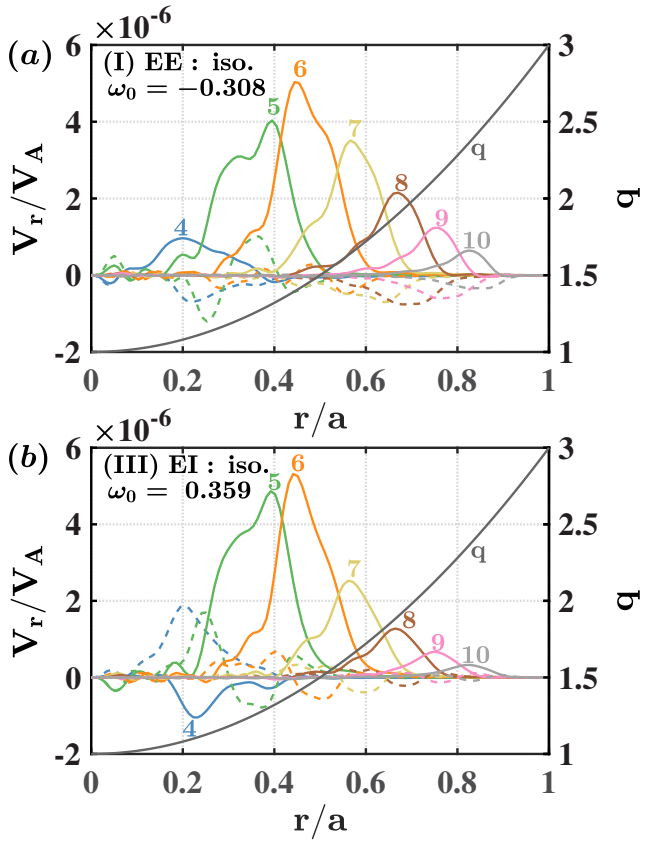

Figure 13. Radial velocity fluctuation profiles of $n = 4$ TAE driven by isotropic Maxwellian (*a*) energetic electrons and (*b*) energetic ions, respectively.

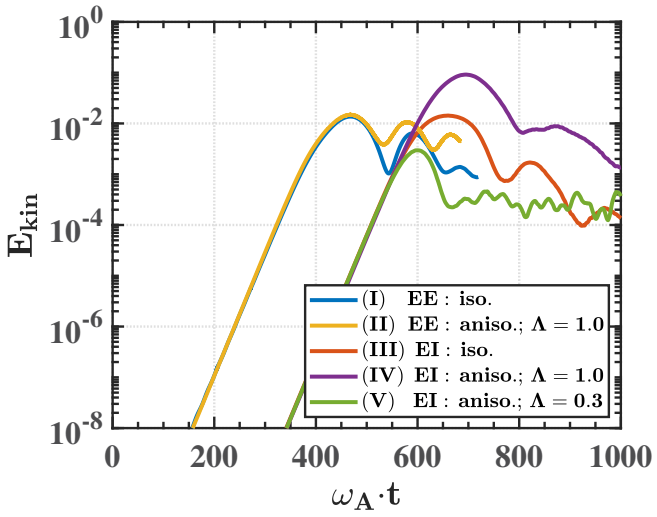

Figure 14. Kinetic energy evolution of $n = 4$ TAE mode for cases (I–V). Detailed numerical parameters for these five cases are listed in table 1.

3.4. Saturation levels of energetic electron/ion driven TAE

In this subsection, we discuss the non-linear saturation levels of energetic electron/ion driven TAE. The similar centrally-peaked energetic particle beta profile, as shown in figure 1, is adopted for both energetic electrons and energetic ions, but different central beta values are chosen so that energetic-electron driven TAE and energetic-ion driven TAE have the same linear growth rate. Other equilibrium profiles and parameters are the same as those in subsection 3.1.

We investigate a total of five runs (cases (I–V)) with different energetic particle distributions. The numerical parameters are listed in table 1. Two of them are energetic-electron simulations using isotropic Maxwellian distribution in case (I) and anisotropic Maxwellian distribution with a peak value at $\Lambda_{peak} = 1.0$ in cases (II), respectively. The remaining three are energetic-ion simulations using isotropic Maxwellian distribution in case (III), anisotropic Maxwellian distribution with a peak value at $\Lambda_{peak} = 1.0$ in case (IV), and anisotropic Maxwellian distribution with a peak value at $\Lambda_{peak} = 0.3$ in case (V), respectively. Apart from the difference in mode frequency, which is listed in table 1, the mode structures are very similar for all five runs. Figure 13 shows the linear structures of $n = 4$ TAE in cases (I) and (III). The mode structure in cases (II), (IV) and (V) are not shown in the figure, because the linear structures of isotropic-energetic-particle driven TAE and anisotropic-energetic-particle driven TAE are almost the same in this work. figure 14 shows the time evolution of MHD kinetic energy for all cases. In cases (I) and (II), TAE driven by energetic electrons with different initial distribution function has the similar saturation level $v_r/v_A \sim 1.0 \times 10^{-3}$. The similar saturation level maybe due to the similar group of resonant energetic electrons in these two cases. Indeed, this saturation amplitude is not very large [31, 51] and the wave-particle trapping is believed to be the main saturation mechanism for cases (I) and (II). In case (III), the saturation level of energetic-ion driven TAE with isotropic Maxwellian distribution is $v_r/v_A \sim 1.4 \times 10^{-3}$, which is slightly higher than the saturation level of energetic-electron driven TAE. However, unlike isotropic Maxwellian energetic electrons in case (I), both passing and trapped energetic ions can significantly drive the mode. Therefore, a lower central energetic particle beta is used in case (III)

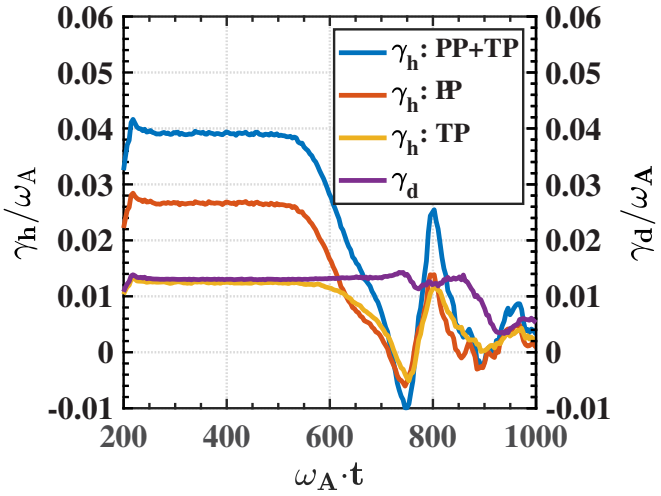

Figure 15. Evolutions of energetic particle driving rate γ_h and system dissipation rate γ_d for case (III).

to drive a TAE with the same growth rate. In order to check the role of passing energetic ions and trapped energetic ions in mode saturation process, cases (IV) and (V) are carried out. It is surprising that trapped-energetic-ion driven TAE in case (IV) and passing-energetic-ion driven TAE in case (V), which have the same linear growth rate, show a large difference in the mode saturation level. In case (IV) with $\Lambda_{\rm peak} = 1.0$, the TAE has a saturation level $v_r/v_A \sim 2.9 \times 10^{-3}$, while the saturation level dramatically decreases to $v_r/v_A \sim 6.5 \times 10^{-4}$ in case (V). The different saturation levels suggest that the bounce frequency of passing energetic ions is larger than that of trapped energetic ions for the TAE with the same amplitude. In other words, passing energetic ions are easier to be trapped in the TAE wave than trapped energetic ions.

To further confirm the difference in particle trapping for passing and trapped energetic ions, we analysed the evolution of energetic particle drive in case (III). The energy evolution of $n = 4$ TAE mode is given by [31]

$$\frac{\mathrm{d}}{\mathrm{d}t}\mathrm{W}_4 = 2\gamma_h(t)\mathrm{W}_4 - \mathrm{D}_4 + \mathrm{N}_4, \tag{10}$$

$$\mathrm{D}_4 = \int \left[\nu\rho\omega_4^2 + \frac{4}{3}\nu\rho\left(\nabla\cdot\boldsymbol{v}_4\right)^2 + \eta\boldsymbol{j}_4\cdot\delta\boldsymbol{j}_4\right]\mathrm{dV}, \tag{11}$$

where $\gamma_h = -\mathrm{P_w}/2\mathrm{W}_4$ represents the energetic-particle driving rate, and N_4 is the energy transfer from the other toroidal mode numbers which is neglected here due to the weak nonlinear coupling. D_4 is the energy dissipation of $n = 4$ mode and the dissipation rate is given by $\gamma_d = \mathrm{D}_4/2\mathrm{W}_4$. Then, the equation (10) is equivalent to $\gamma_L = \gamma_h - \gamma_d$, where γ_L is the mode growth rate. Figure 15 shows the time evolution of passing/trapped energetic ion driving rate and mode dissipation rate. The saturation occurs at the cross point of the total driving rate and dissipation rate around $\omega_A t = 660$ in the figure. During linear phase, about 68% of the total drive comes from passing energetic ions and the rest comes from trapped energetic ions. The driving rate from passing energetic ions starts to fall at $\omega_A t = 520$. The driving rate from trapped energetic ions starts to fall at a later moment around $\omega_A t = 580$. This confirms that the particle trapping happens at a higher TAE amplitude for trapped energetic ions.

4. Summary

In this paper, the energetic-electron driven AEs were investigated via hybrid simulations of an MHD fluid interacting with energetic electrons. A quantitative analysis of energetic electron drive in AE destabilization was presented in terms of the particle orbit type and the phase space position. Energetic electrons with beta profiles both peaked on-axis and off-axis are considered. For the on-axis peaked energetic electron beta profile or off-axis peaked energetic electron beta profile with $\partial f/\partial r < 0$, an unstable $n = 4$ TAE propagating in the electron diamagnetic drift direction was found. The mode frequency of the destabilized TAE increases with the increase of initial energetic electron energy. Deeply trapped energetic electrons are responsible for the mode destabilization through precession resonance with the resonance number $L = 0$. In on-axis peaked beta profile case, about 90% of the total drive comes from trapped energetic electrons. The rest drive comes from passing energetic electrons. A few passing energetic electrons spatially localized around the rational surfaces were found that can resonate with the TAE due to the small value of $k_{\|}$ near the rational surface. For TAE driven by isotropic Maxwellian energetic electrons and anisotropic Maxwellian ($\Lambda_{\rm peak} = 1.0$) energetic electrons with the same linear growth rate, the mode structure, frequency, and saturation level are all similar. Besides, a TAE driven by isotropic Maxwellian energetic ions with the same linear growth rate also shows a similar saturation level. Moreover, for TAE driven by anisotropic Maxwellian energetic ions, the trapped-energetic-ion-driven TAE shows a larger saturation level than the passing-energetic-ion-driven TAE, which indicates that passing energetic ions are easier to be trapped in the TAE wave than trapped energetic ions. For the off-axis peaked energetic electron beta profile with $\partial f/\partial r > 0$, an unstable $n = 4$ EAE-type EPM propagating in the ion diamagnetic drift direction was found when a safety factor profile with weak magnetic shear at the mode center was adopted. The main poloidal harmonics are $m = 6$ and $m = 8$, and mode frequency is near the second Alfvén frequency gap. This positive frequency AE was driven by passing energetic electrons with the resonance number $L = \pm 7$ and barely trapped energetic electrons with the resonance number $L = 0$. The flat $q-$profile enables a lot of passing energetic electrons near the mode center resonating with the mode.

More generally, for the energetic-electron-driven TAE, deeply trapped energetic electrons are responsible for the destabilization of TAE propagating in the electron diamagnetic drift direction, while barely trapped energetic electrons are expected to be responsible for the destabilization of TAE propagating in the ion diamagnetic drift direction although we failed to destabilize this kind of TAE in the present simulation. On the other hand, we found that the passing energetic electron could not dominate the TAE destabilization. This is consistent with the reported experiments that TAE can be driven

in an ECRH plasma or a lower-hybrid-wave-driven plasma, and not in an ECCD plasma. For the energetic-electron-driven EAE or EAE-type EPM, the role of the trapped energetic electron would not be altered, but the role of the passing energetic electron will be quite different. We found that passing energetic electrons can dominate the destabilization of an EAE-type EPM, which indicates the destabilization of EAE/EAE-type EPM by ECCD is possible in experiments. Such kind of destabilization process is mainly restricted to the local magnetic shear around the mode center and is not restricted to the specific particle velocity, pitch angle value or mode propagation direction. Although many aspects of the interaction between energetic electrons and AEs have been discussed in this work, a further study related to TAE driven by barely trapped energetic electrons is required in order to fully unravel the destabilization mechanism of AE by energetic electrons. We believe that adopting a more realistic energetic electron distribution generated by LH wave or high field side ECRH will help to achieve this kind of instability.

The relativistic effect deserves to be addressed for energetic-electron-driven AE, because we noticed that the kinetic energy of resonant trapped energetic electrons is relatively high in both experiment and our simulation. For example, the observed $n=4$ TAE in HL-2A was driven by energetic electrons with energy in the range of $150-230$ keV [24]. In our simulation, if we consider a TFTR plasma: $a=0.85$ m, $R_0=2.72$ m, $B_0=1.25$ T, and the bulk (deuterium) ion density $n_i=1.9\times10^{19}\,\mathrm{m}^{-3}$, which is consistent with the numerical setup, the kinetic energy of a resonant trapped energetic electron with $E=0.5\,m_\mathrm{D}v_A^2$ (or $v_\mathrm{EE}=61\,v_A$) will be 106 keV. Such resonant energetic electrons require a relativistic correction of 30 %. The corresponding change of particle mass will alter the particle orbit frequencies and drift orbit width, affecting the resonance condition somewhat, but such change is not expected to alter the conclusion of present work. However, the relativistic effect should be considered when investigating the energetic-electron-driven AE with very low toroidal mode number n, like $n=1$ and $n=2$.

4. Acknowledgments

This work was supported by the National Natural Science Foundation of China with No. 11675038 and the National Key R&D Program of China (Grant No. 2017YFE0301900). Numerical computations were performed on the Plasma Simulator (FUJITSU FX100) of NIFS with the support and under the auspices of the NIFS Collaboration Research program (NIFS18KNST125, NIFS19KNXN396), and on the JFRS-1 of the International Fusion Energy Research Center. J. Wang thanks the China Scholarship Council (CSC), as the present study was completed during his visit to National Institute for Fusion Science (NIFS) sponsored by CSC (No. 201706060116).

ORCID iDs

Jialei Wang https://orcid.org/0000-0002-8678-8075
Yasushi Todo https://orcid.org/0000-0001-9323-8285
Hao Wang https://orcid.org/0000-0002-9819-7483

References

[1] Rosenbluth M.N. and Rutherford P.H. 1975 *Phys. Rev. Lett.* **34** 1428
[2] Cheng C.Z. and Chance M.S. 1986 *Phys. Fluids* **29** 3695
[3] Heidbrink W.W. 2008 *Phys. Plasmas* **15** 055501
[4] Chen L. 1994 *Phys. Plasmas* **1** 1519
[5] Chen L. and Zonca F. 2016 *Rev. Mod. Phys.* **88** 015008
[6] Todo Y. 2019 *Rev. Mod. Plasma Phys.* **3** 1
[7] Fasoli A. *et al* 2007 Progress in the ITER Physics Basis Chapter 5: Physics of energetic ions *Nucl. Fusion* **47** S264
[8] Toi K. *et al* 2011 *Plasma Phys. Control. Fusion* **53** 024008
[9] Sharapov S. *et al* 2013 *Nucl. Fusion* **53** 104022
[10] Gorelenkov N., Pinches S. and Toi K. 2014 *Nucl. Fusion* **54** 125001
[11] Van Zeeland M.A. *et al* 2012 *Nucl. Fusion* **52** 094023
[12] Bierwage A. *et al* 2018 *Nat. Commun.* **9** 3282
[13] Fu G.Y. and Van Dam J.W. 1989 *Phys. Fluids B* **1** 1949
[14] Berk H.L. and Breizman B.N. 1990 *Phys. Fluids B* **2** 2226
[15] Wang X., Zonca F. and Chen L. 2010 *Plasma Phys. Control. Fusion* **52** 115005
[16] Wang Z. *et al* 2013 *Phys. Rev. Lett.* **111** 145003
[17] Zhu J., Ma Z.W. and Wang S. 2016 *Phys. Plasmas* **23** 122506
[18] Yang S.X. *et al* 2018 *Nucl. Fusion* **58** 046016
[19] Zonca F. 2007 *et al Nucl. Fusion* **47** 1588
[20] Vlad G. *et al* 2016 *New J. Phys.* **18** 105004
[21] Valovič M. *et al* 2000 *Nucl. Fusion* **40** 1569
[22] Chen W. *et al* 2010 *Phys. Rev. Lett.* **105** 185004
[23] Ding X.T. *et al* 2013 *Nucl. Fusion* **53** 043015
[24] Yu L.M. *et al* 2018 *Phys. Plasmas* **25** 012112
[25] Snipes J.A. *et al* 2008 *Nucl. Fusion* **48** 072001
[26] Hu W. *et al* 2018 *Nucl. Fusion* **58** 096032
[27] Chu N. *et al* 2018 *Nucl. Fusion* **58** 104004
[28] Cheng J. *et al* 2016 *Phys. Plasmas* **23** 052504
[29] Todo Y. and Sato T. 1998 *Phys. Plasmas* **5** 1321
[30] Todo Y. 2006 *Phys. Plasmas* **13** 082503
[31] Todo Y., Berk H.L. and Breizman B.N. 2010 *Nucl. Fusion* **50** 084016
[32] Todo Y. 2016 *New J. Phys.* **18** 115005
[33] Todo Y., Berk H.L. and Breizman B.N. 2012 *Nucl. Fusion* **52** 033003
[34] Park W. *et al* 1992 *Phys. Fluids B* **4** 2033
[35] Spong D.A., Carreras B.A. and Hedrick C.L. 1994 *Phys. Plasmas* **1** 1503
[36] Briguglio S., Vlad G., Zonca F. and Kar C. 1995 *Phys. Plasmas* **2** 3711
[37] Chen Y. *et al* 2010 *Phys. Plasmas* **17** 102504
[38] Littlejohn R.G. 1983 *J. Plasma Phys.* **29** 111
[39] Könies A. *et al* 2018 *Nucl. Fusion* **58** 126027
[40] Wang H. *et al* 2018 *Phys. Rev. Lett.* **120** 175001
[41] Seki R. *et al* 2019 *Nucl. Fusion* **59** 096018
[42] Sato M. and Todo Y. 2019 *Nucl. Fusion* **59** 094003
[43] Bierwage A. *et al* 2017 *Nucl. Fusion* **57** 016036
[44] Todo Y. *et al* 2014 *Nucl. Fusion* **54** 104012
[45] Todo Y. 2012 *AIP Conf. Proc.* **1478** 141
[46] Chu M.S. *et al* 1992 *Phys. Fluids B* **4** 3713
[47] Chen W. *et al* 2009 *Nucl. Fusion* **49** 075022
[48] Chen W. *et al* 2010 *Nucl. Fusion* **50** 084008
[49] White R.B. 2001 *The Theory of Toroidally Confined Plasmas* 2nd edn ch 3 (London: Imperial College Prress)
[50] Zonca F. and Chen L. 1992 *Phys. Rev. Lett.* **68** 592
[51] Rosenbluth M.N. *et al* 1992 *Phys. Rev. Lett.* **68** 596
[52] Berk H.L., Breizman B.N. and Pekker M.S. 1995 *Nucl. Fusion* **35** 1713
[53] Fu G.Y. and Park W. 1995 *Phys. Rev. Lett.* **74** 1594